

LRS Bianchi Type-I Cosmological Model in Self Creation Theory of Gravitation

M. Vijaya Santhi^{*1}, D. CH. Paparao², T. Chinnappalanaidu¹, S. Srivani Madhu¹,

¹Department of Applied Mathematics, Andhra University, Visakhapatnam 530003, India

²Department of Mathematics, V.K.V. Government Degree College, Kothapeta, A.P., India

*gv.sanathi@live.com

Article Info

Page Number: 1073 – 1090

Publication Issue:

Vol. 71 No. 3s2 (2022)

Article History

Article Received: 28 April 2022

Revised: 15 May 2022

Accepted: 20 June 2022

Publication: 21 July 2022

Abstract

We have examined LRS Bianchi type-I space-time in the continuance of Barrow holographic dark energy, for the self-creation theory in this following article. In order to derive an accurate solution to the field equations, we put forth metric potentials relation as $A = B^n$ and equalizing the sum of the trace of the energy momentum tensor to zero as $T + \bar{T} = 0$. Further, we have observed the physical behavior of some important cosmological parameters like deceleration q , statefinder (r, s) EoS (ω_{de}) , $(\omega_{de} - \omega_{de}')$ plane, skewness parameter (δ) , squared speed of sound (v_s^2) that analyzes the model's stability. Also, study of cosmographic parameters $(j, s \& l)$ and density parameter (Ω_{de}) has been conducted and we could conclude that these parameters are in obedience with the current observational data. The model thus obtained has a stable behavior; and shows quintessence nature and that the Universe is expanding in an accelerated manner.

Keywords: LRS Bianchi type-I metric, Self-creation theory, Borrow holographic dark energy, Holographic dark energy, Dark energy, Density parameter.

1 Introduction

Scientists have revealed a new map of the early Universe that clarifies a long-standing puzzle over the ongoing expansion of the cosmos, as predicted from the cosmic microwave background (CMB) data of ACT experiments [1, 2]. The discrepancy of Hubble constant, as named after the US astronomer Edwin Hubble, is being used as a tool by the cosmologists to estimate the Universe's expansion rate. Many astonishing facts about the cosmic evolution has been put forward from constructing various cosmological model and state-of-the-art CMB maps provided from Planck's Mission, acts as a backbone to know about the structure and nature of the cosmos [3]. By presuming the standard cosmological model as true, Planck's data [4] calculations predicts accurately how rapidly the cosmos is expanding now. Nonetheless, over the past decennium it has been observed that there is 5-10% faster expansion and this has been affirmed from more detailed measurements of the expansion, based on the Supernova explosions [5, 6] and other mechanisms. As said by many theorists, we are far from totally comprehending the mysterious dark force named, as the Dark Energy (DE) which consists of 68% of the Universe, which is accountable for the cosmic expansion. And, equally mysterious dark matter (DM) (around 27%) is the principle reason for the formation of galaxies and is the invisible force that holds the galaxies and the cosmic web.

The ordinary matter constitutes for less than 5% of total mass and energy of the cosmos. There has been considerable amount of knowledge about the DM, ever since its existence has been suggested in early 1920's. However, DE has come into light only after 1998, that is detected from observing the gravitational interactions. And on large scales, the gravitational effect of DE is repulsive, pushing things away from each other and making the Universe's expansion hasten. Having said that, at the early phases, the DE might not be strong enough to carryout an accelerated expansion; rather it would have caused the plasma that appeared after the Big Bang to cool down faster than it would have otherwise. As a result, the interpretation of CMB data may be affected, particularly when it comes to measure the Universe's age and its expansion rate, which rely on the amount of sound waves that could travel through the plasma before it cooled into gas [7].

As a compelling way to interpret DE, the Holographic principle [8–13] and Holographic dark energy (HDE) gives some interesting cosmological frameworks that are simple and as well as extended versions, depending on the utility of the horizons, as the Universe's radius accede with the contemporary observations. Here, the inequality $\rho_{de}L^4 \leq S$ represents the standard HDE, with L as the horizon length, ρ_{de} as energy density and S the entropy. And under the imposition $S \propto A \propto L^2$ [14], there is the use of Barrow entropy

$$S_B = \left(\frac{B}{B_0}\right)^{1+\frac{\Delta}{2}}, \quad \text{for } 0 \leq \Delta \leq 1, \quad (1)$$

where B and B_0 respectively represent the standard horizon and the Planck area; as an alternative to the regular Bekenstein-Hawking one [15–18], which eventually lead to

$$\rho_d = CL^{\Delta-2}, \quad (2)$$

with C as a parameter with dimensions $[L]^{-2-\Delta}$. In order to describe the quantum-gravitational deformation, a new exponent is hence introduced that is quantified as Δ . As expected, the above expression provides the standard HDE whenever $\Delta = 0$, i.e. $\rho_d = 3c^2M_p^2L^{-2}$, where C takes the value as $C = 3c^2M_p^2$, with M_p as the Planck mass and c^2 as the model parameter. On the other hand, when the deformation effects, as quantified by Δ occurs, the Barrow holographic dark energy (BHDE) departs from the standard model, giving a different cosmological behavior. However, researches have developed interests to use the BHDE model and many recent studies have been performed, of which some are mentioned here. The anisotropic Bianchi Type (BT)-I Universe with BHDE and matter have been investigated by Paul et al. [19]. In a study by Mannon et al. [20], they looked at how a FLRW Universe evolves when pressureless DM and BHDE interact through a well-motivated interaction term. To analyze the evolutionary history of essential cosmological parameters Remya and sharma [21] have researched the advancement of the FRW Universe filled with pressureless DM and BHDE density by using the Hubble horizon as the IR cutoff. Adhikary et al.[22] have constructed BHDE in the case of nonflat Universe. In the framework of the DGP braneworld model Rani and Azhar [23] have investigated the evolution of the cosmic parameters and planes with the interaction between the BHDE and pressureless DM. Bhardwaj et al. [24] have discussed statefinder hierarchy for BHDE model in the FLRW Universe.

As elucidated by Hubble's law [25-27], there is moving away of galaxies from each other in all directions as endorsed by their redshift. A remarkable study has observed that the rate of

this expansion manifests that the Universe is approaching to the critical density, and this is responsible for this expansion forever. It is accustomed to express the density as a fraction of the average density of matter and energy of the Universe to the density required for the 'critical condition', which is defined as the density at which the Universe would stop expanding only after an infinite time. Therefore, the density parameter is given by

$$\Omega_{de} = \frac{\rho}{\rho_c} = \frac{8\pi G\rho_{de}}{3H^2}, \quad (3)$$

where ρ is the actual density, ρ_c is the critical density and $\rho_c = \frac{3H^2}{8\pi G}$.

The sum of the contributions to the total density parameter (Ω_{de}) at the current time is $\Omega_{de} = 1.02^{+0.02}_{-0.02}$, indicating that the Universe is very close to critical density or $\Omega_{de} = 1$. Even after knowing that Ω_{de} is very close to 1 by the on going experiments, the overall future of the Universe is subjected to the values of Ω_{de} , whether it is slightly greater than 1, less than 1, or exactly equal to 1.

- For $\Omega_{de} < 1$: Universe is open and continues to expand thereafter.
- For $\Omega_{de} > 1$: Universe is closed and eventually halts its expansion and recollapses.
- For $\Omega_{de} = 1$: Universe is flat and constitutes enough matter to halt the expansion but not sufficient to recollapse it.

Despite the prominence of General theory of Relativity (GR) [28-32], the Mach principle has not been substantiated by GR. Therefore, a need arises to incorporate Mach's principle and other necessary features that are absent in the primary theory, by generalizing the Einstein's GR. Jordan and then Brans and Dicke has initially proposed an alternative to GR, called as the scalar-tensor theories, which Barber has modified and proposed two self-creation theories (SCT) [33]. The first SCT is a modification to Brans-Dicke theory [34]. However, it is not applicable as it does not comply with equivalence principle. An adoption of GR is the second proposal. It includes continuous creation within limits of observations. Many recent works have been done in this framework, of which the following are few. Kantowski-Sachs cosmological model has been investigated by Ram et al. [35], in the presence of an anisotropic modified Ricci DE within the framework of Barber's second SCT. Geometrical and physical aspects of the LRS BT-II metric with string viscous fluid have been evaluated by Ashtankar et al. [36], on solving the barber's field equations of second SCT. Jain and Jain [37] have constructed DE cosmological model in an anisotropic BT-VI₀ space time with a variable equation of state (EoS) parameter ω in Barber's SCT. Chauhan [38] has studied LRS BT-I metric by using variable deceleration parameter and has investigated the field equations of Barber's second SCT with perfect fluid source. Wet dark fluid BT-VIII cosmic model in Barber's SCT has been investigated by Wankhade et al. [39]. By assuming that Universe is filled with barotropic fluid distribution Advani [40] has studied BT-V in perfect fluid and Lyra geometry with SCT. BT-I cosmological model in Lyra geometry and Barber's second SCT with disordered radiation have been discussed by Advani and Jain [41].

This work has been divided into following sections. Section (2), is concerned with the derivation of field equations and we find the solution for the model using certain conditions. Some geometrical properties of the model have been studied in the section (3). In the last section (4) we have interpreted the properties of the model and drawn some conclusions from this work.

2 Mathematical formalism of the model

Bianchi I – IX cosmological models has a vital role in the study of the Universe, as they are homogeneous and anisotropic, and this allows us to understand the method of isotropization of the Universe as the time passes. Furthermore, theoretically it is observed that FRW isotropic models has less generality when compared to anisotropic Universe. Bianchi space-times help constructing spatially homogeneous and anisotropic models because of the easiness of the field equations. Considerable amount of work has been done in obtaining various BT cosmological models. Kumar and Arora [42] have investigated a cosmological model employing a four-degree function of cosmic time t in the $f(R, T)$ gravity theory using an extended form of deceleration parameter. The spatially homogeneous and anisotropic BT and axially symmetric model have been studied by Dixit et al. [43], that is filled with DM and DE in Brans-Dicke theory of gravitation. Study of a BT-I cosmos with barotropic and DE type fluids has been studied by Goswami et al. [44]. The paper titled “Constraining BT-I Universe with type Ia supernova and $H(z)$ data” is the work of Amirhashchi and Amirhashchi [45]. Singla et al. [46] have examined the existence of BT-I Brans–Dicke theory by performing statistical test from $H(z)$ and SuperNovae Ia experimental sets. Very recently, using a BT-I geometry coupled to the Kalb–Ramond field has been investigated by Maluf and Neves [47]. Therefore, the spatially homogeneous BT-I metric of the form

$$ds^2 = A^2 dx^2 + B^2(dy^2 + dz^2) - dt^2, \quad (4)$$

where metric potentials A, B are functions of t only, has been contemplated.

Also, Barber’s SCT has the following field equations,

$$R_{ij} - \frac{1}{2}Rg_{ij} = -8\pi\phi^{-1}(T_{ij} + \bar{T}_{ij}), \quad (5)$$

$$\& \quad \square\phi = \phi_{;v}^v = \frac{8\pi}{3}\mu(T + \bar{T}), \quad (6)$$

where the Ricci tensor, the Ricci scalar, energy momentum tensor of matter, the energy momentum tensor of BHDE and the coupling constant are given as R_{ij} , R , T_{ij} , \bar{T}_{ij} and μ respectively. The energy momentum tensors for pressureless matter and anisotropic DE are given by

$$T_{ij} = \text{diag}[0,0,0, \rho_m], \quad (7)$$

$$\bar{T}_{ij} = \text{diag}[\rho_{de}\omega_{de}, \rho_{de}\omega_{de}, (\omega_{de} + \delta)\rho_{de}, -\rho_{de}], \quad (8)$$

where $\omega_{de} = \frac{p}{\rho_{de}}$ is equation of state (EoS) parameter of DE, p and ρ_{de} are pressure and energy density of DE respectively. ρ_m is the energy density of the matter and δ is the deviation (skewness parameter) from ω_{de} in z direction.

Now in the co-moving coordinate system, the field equations (5) and (6) for the metric (4), using Eq.(7) can be deduced as,

$$\frac{2\ddot{B}}{B} + \left(\frac{\dot{B}}{B}\right)^2 = \frac{-8\pi\rho_{de}\omega_{de}}{\phi}. \quad (9)$$

$$\frac{\ddot{A}}{A} + \frac{\ddot{B}}{B} + \frac{\dot{A}\dot{B}}{AB} = \frac{-8\pi\rho_{de}\omega_{de}}{\phi}. \quad (10)$$

$$\frac{\ddot{A}}{A} + \frac{\ddot{B}}{B} + \frac{\dot{A}\dot{B}}{AB} = \frac{-8\pi(\omega_{de} + \delta)\rho_{de}}{\phi}. \quad (11)$$

$$2 \frac{\dot{A}\dot{B}}{AB} + \left(\frac{\dot{B}}{B}\right)^2 = \frac{8\pi(\rho_{de} + \rho_m)}{\phi} \tag{12}$$

$$\ddot{\phi} + \dot{\phi} \left(\frac{\dot{A}}{A} + 2\frac{\dot{B}}{B}\right) = \frac{8\pi\mu(T + \bar{T})}{3} \tag{13}$$

Here the over head dot denotes the differentiation with respect to ‘t’. To obtain the values of the unknowns namely, A, B, ϕ , ρ_m , ρ_{de} , ω_{de} , and δ from the five field equations (9)-(13), we can consider the metric potentials relation by taking proportionality between the shear scalar (σ) and expansion scalar (θ) (Collins et al. [48]) as $A = B^n$, (14)

where $n > 0, (\neq 1)$ is a constant and preserves the anisotropic character of the space-time; and equalizing the sum of the trace of the energy momentum tensor to zero as

$$T + \bar{T} = 0. \tag{15}$$

The expressions for metric potentials can be obtained by using Eqs. (11),(9), (14) and (15) as

$$A = ((n + 2)e^{\gamma_1 t} + (n + 2)\gamma_2)^{\frac{n}{n+2}}, \tag{16}$$

$$B = ((n + 2)e^{\gamma_1 t} + (n + 2)\gamma_2)^{\frac{1}{n+2}}, \tag{17}$$

and the scalar field ϕ as

$$\phi = c_2 - \frac{c_1}{(n+1)((n+2)e^{\gamma_1 t} + (n+2)\gamma_2)^{\frac{n+1}{n+2}}}. \tag{18}$$

Therefore, Eq. (4) is modified to,

$$ds^2 = ((n + 2)e^{\gamma_1 t} + (n + 2)\gamma_2)^{\frac{2n}{n+2}} dx^2 + ((n + 2)e^{\gamma_1 t} + (n + 2)\gamma_2)^{\frac{2}{n+2}} (dy^2 + dz^2) - dt^2. \tag{19}$$

Here, Eq. (19) represents a four-dimensional anisotropic BT-I cosmic model with BHDE in SCT with the physical and geometrical parameters discussed in the next section, which has prominence in the astronomical studies. Now, the cosmological parameters like volume (V), average scale factor (a(t)), Hubble parameter (H), expansion scalar (θ), shear scalar (σ^2) and anisotropic parameter (\mathcal{A}_h) of the BT-I cosmic model are defined as,

$$V = (n + 2)(e^{\gamma_1 t} + \gamma_2), \tag{20}$$

$$a = ((n + 2)(e^{\gamma_1 t} + \gamma_2))^{\frac{1}{3}}, \tag{21}$$

$$H = \frac{\gamma_1 e^{\gamma_1 t}}{3e^{\gamma_1 t} + 3\gamma_2}, \tag{22}$$

$$\theta = \frac{\gamma_1 e^{\gamma_1 t}}{e^{\gamma_1 t} + \gamma_2}, \tag{23}$$

$$\sigma^2 = \frac{\gamma_1^2 e^{2\gamma_1 t}}{3(n+2)^2 (e^{\gamma_1 t} + \gamma_2)^2}, \tag{24}$$

$$\text{and } \mathcal{A}_h = \frac{2(n-1)^2}{(n+2)^2}. \tag{25}$$

From Eqs. (20)-(24), we observe that, initially (i. e. $t = 0$) the spatial volume (V), scale factor (a), Hubble parameter (H), shear scalar (θ) and expansion scalar (σ^2) become constants. However, they tend to infinity as $t \rightarrow \infty$. Also, from Eq. (25), we observe that the anisotropic parameter (\mathcal{A}_h) $\neq 0$, throughout the evolution of the Universe, which indicates that the model (19) is anisotropic.

The energy density of BHDE is given by

$$\rho_{de} = \frac{9C(e^{\gamma_1 t} + \gamma_2)^2 e^{-2\gamma_1 t} 3^{-\Delta} \left(\frac{e^{\gamma_1 t} \gamma_1}{e^{\gamma_1 t} + \gamma_2}\right)^\Delta}{\gamma_1^2}. \tag{26}$$

The following expression represents energy density of matter as,

$$\rho_m = \frac{\Psi_1}{8\pi(n+2)^2(e^{\gamma_1 t + \gamma_2})^2(n+1)\gamma_1^2} \tag{27}$$

where,

$$\Psi_1 = \left. \begin{aligned} & -2e^{2\gamma_1 t} \left(n + \frac{1}{2}\right) \gamma_1^4 c_1 \left((n+2)(e^{\gamma_1 t} + \gamma_2)\right)^{\frac{-n-1}{n+2}} + 2(n+1) \left(-36e^{-2\gamma_1 t} 3^{-\Delta} \pi C(n+2)^2 \times \right. \\ & \left. (e^{\gamma_1 t} + \gamma_2)^4 \left(\frac{e^{\gamma_1 t} \gamma_1}{e^{\gamma_1 t} + \gamma_2}\right)^\Delta + e^{2\gamma_1 t} c_2 \gamma_1^4 \left(n + \frac{1}{2}\right) \right) \end{aligned} \right\}$$

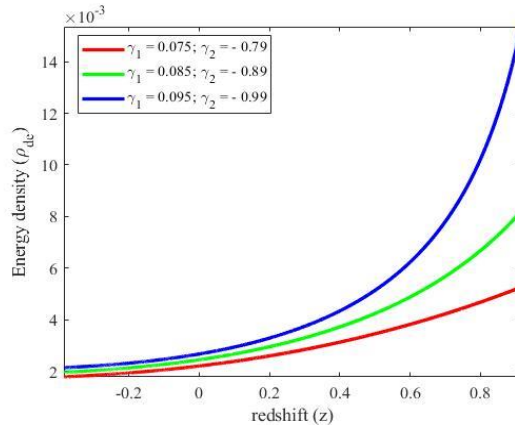


Figure 1: Illustration of energy density(ρ_{de}) against redshift(z).

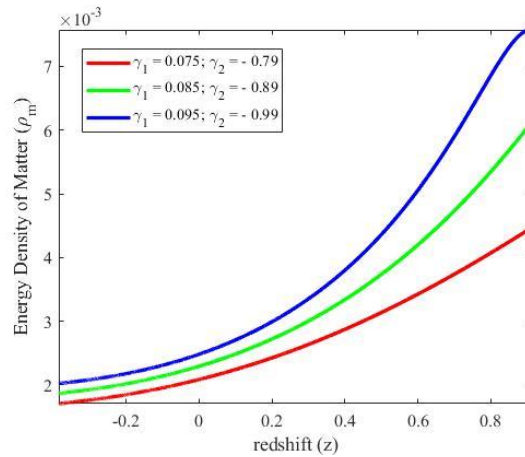


Figure 2: Illustration of energy density matter(ρ_m) against redshift(z).

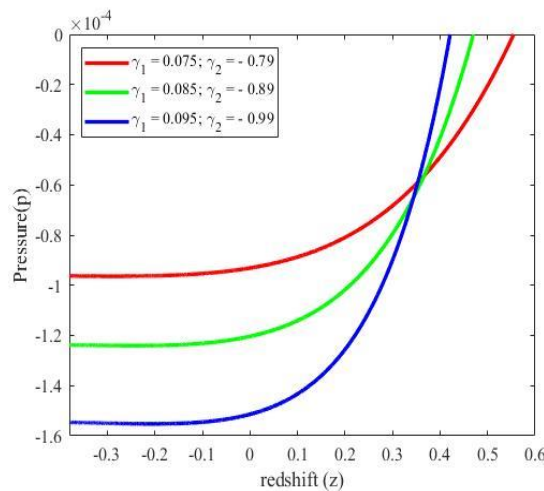


Figure 3: Illustration of pressure(p) against redshift(z).

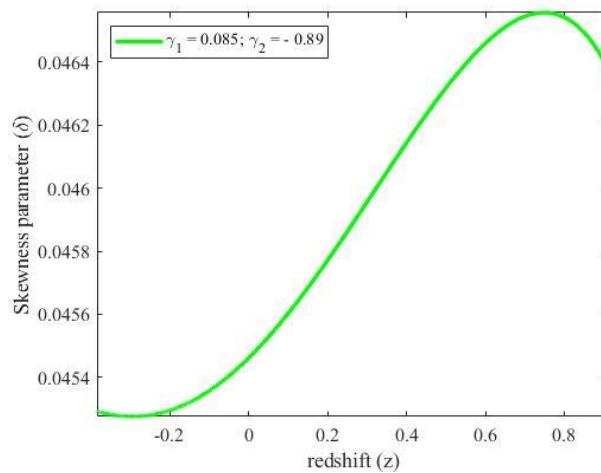


Figure 4: Illustration of skewness parameter (δ) against redshift (z)

The pressure of BHDE and the skewness parameter are given by,

$$p = \frac{\gamma_1^2((n^2+n+4)e^{2\gamma_1 t} + e^{\gamma_1 t}\gamma_2(n+3)(n+2))((n+2)(e^{\gamma_1 t} + \gamma_2))^{\frac{-n-1}{n+2}} c_1 - c_2 n - c_2}{16\pi(n+2)^2(e^{\gamma_1 t} + \gamma_2)^2(n+1)}, \tag{28}$$

$$\delta = \frac{(n-1)((n+2)(e^{\gamma_1 t} + \gamma_2))^{\frac{-n-1}{n+2}} c_1 - c_2(n+1)3^{\Delta}\gamma_1^4\left(\frac{e^{\gamma_1 t}\gamma_1}{e^{\gamma_1 t} + \gamma_2}\right)^{-\Delta}e^{3\gamma_1 t}}{72(n+2)\pi C(e^{\gamma_1 t} + \gamma_2)^3(n+1)}. \tag{29}$$

From figures (1) and (2), we observe that ρ_{de} and ρ_m , for various values of γ_1 & γ_2 varies in positive region, decreasing against redshift (z) respectively. And the trajectories of pressure of BHDE against redshift (z) are plotted in figure (3) for the various values of γ_1 & γ_2 . The curves varies in negative region and are decreasing against redshift (z). Therefore, we can conclude that the trajectories in the figures (1)-(3) project the accelerated expansion of the cosmos. For our model, the skewness parameter (δ) as defined by the Eq. (29), is depicted in the figure (4). The parameter varies in positive region without vanishing, throughout its evolution for the chosen values of γ_1 & γ_2 .

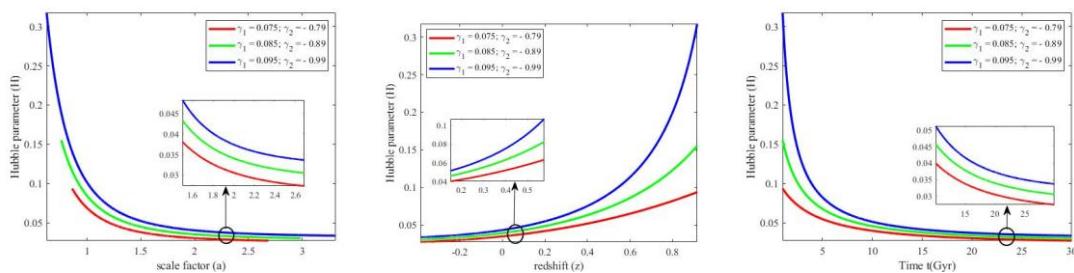


Figure 5: Illustration of Hubble parameter(H) against scale factor(a) (left panel), redshift(z) (center panel) and time(Gyr) (right panel).

Figure (5) are the trajectories of Hubble parameter taken against scale-factor (a), time (t) and redshift (z) respectively. As shown, Hubble parameter shows inverse proportionality towards scale-factor (a) (as shown in left panel), illustrating the cosmic expansion rate. Whereas, there is a direct proportionality between the Hubble parameter (H) and redshift (z) and Hubble parameter attains its present values H_0 at $z = 0$ (as shown in center panel). Also, the Hubble parameter is directly proportional to cosmic time (t) (as shown in right panel).

3 Dynamical behavior of the framework

In this segment, we compute the cosmological parameters such as deceleration (q), statefinder pair ($r - s$ & $q - r$), cosmographic parameters: jerk (j), snap (s) & lerk (l), EoS (ω_{de}), $\omega_{de} - \omega_{de}'$ plane, squared speed of sound (v_s^2) and density parameter (Ω_{de}) for the model (19) and present their physical significance.

• **Deceleration Parameter (q):** An important aspect of cosmological modeling is the explanation for the current acceleration of the Universe and the progress from the decelerating past to the current acceleration by using varying deceleration parameter for anisotropic or isotropic Universe models [49,50]. Deceleration parameter denotes the rate at which the Universe's expansion is slowing down and is given as $q = -(1 + \frac{\ddot{H}}{H^2})$.

Depending on the range of q the expansion of the Universe can be understood [51,52] such as,

- Decelerating expansion when $q > 0$,
- Expansion with constant rate when $q = 0$,
- Accelerating power law expansion when $-1 < q < 0$,
- Exponential expansion/de Sitter expansion when $q = -1$ and
- Super-exponential expansion when $q < -1$.

For the constructed model, deceleration parameter q takes the value as follows:

$$q = \frac{-7\gamma_2^2 - 3e^{-\gamma_1 t} \gamma_2^3 - e^{2\gamma_1 t} - 5e^{\gamma_1 t} \gamma_2}{(e^{\gamma_1 t} + \gamma_2)^2} \tag{30}$$

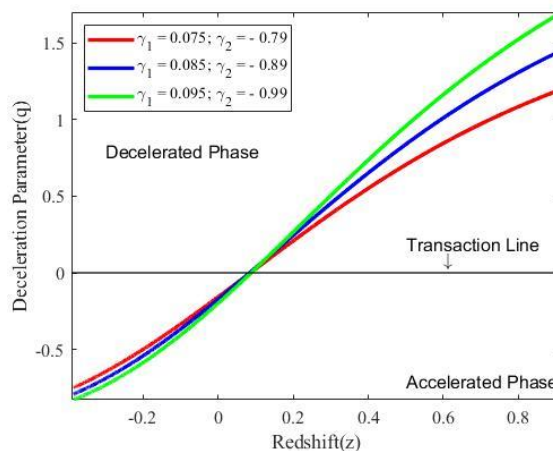


Figure 6: Illustration of deceleration parameter(q) against redshift(z).

The deceleration parameter curve contrasted with redshift (z) for three distinct values of γ_1 & γ_2 respectively, as shown in figure (6) describes that the erstwhile phase of the Universe showed decelerated expansion as the curve transcends from $q > 0$ to $q < 0$ i.e. from decelerated phase to accelerated one, indicating an expansion in accelerating way in the present epoch. These observations are in concurrent with the recent astronomical observations.

• **Statefinder Parameters ($r - s$):** Statefinder parameters are the diagnostic and sensitive tool, given as

$$r = \frac{\ddot{a}}{aH^3} \text{ and } s = \frac{r-1}{3(q-\frac{1}{2})}$$

that differentiates among various DE models, as the degeneracy of the Hubble parameter (H) and the deceleration parameter (q) does not show any difference among different DE models. In this discourse, this geometrical statefinder diagnostic tool that discriminates DE models have been introduced by Sahni et al. [53, 54]. Several authors have researched HDE models in non-flat Universe [55] by considering this statefinder diagnostic. We have characterized the statefinder plane as,

$$r = 1 + 9e^{-2\gamma_1 t} \gamma_2^2 ; \quad s = \frac{-2\gamma_2^2 e^{-\gamma_1 t}}{2\gamma_2 + e^{\gamma_1 t}} \tag{31}$$

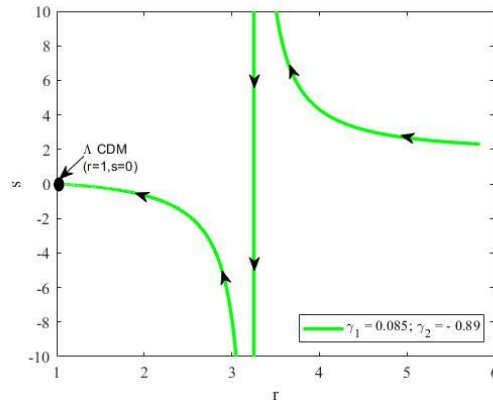


Figure 7: Illustration of (r – s) plane.

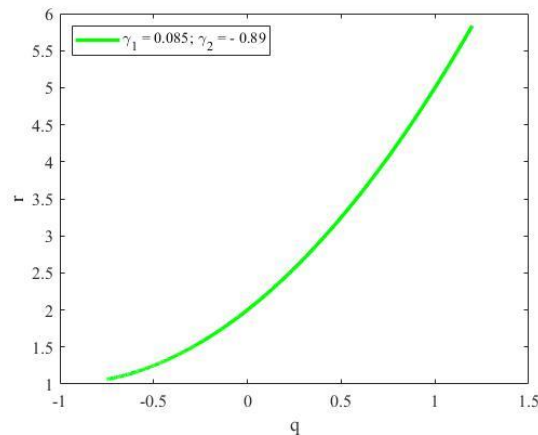


Figure 8: Illustration of (q – r) plane.

The behavior of statefinder parameters $r - s$ and $r - q$ planes are observed from figures (7) and (8) respectively when plotted opposite to redshift (z) for various values of γ_1 & γ_2 . It is clear from figure (7) that the $r - s$ plane trajectories begin from Chaplygin gas region ($r > 1, s < 0$) and passes through the Λ CDM point. At this particular point, our constructed model of the Universe behaves like a Λ CDM model. The trajectories of $r - q$ plane, as recognized from figure (8) vary from positive to negative region, illustrating that the phase transition of the Universe appears in the matter dominated phase and evolves to de-sitter phase.

- **Cosmographic Parameters:** The study of a scale factor (a) with the expansion of the Taylor series w.r.t the cosmic time (t) is called as cosmography. The expansion is independent of the solution of the motion equations of the models and also gives us a relation

between distance and redshift. To study cosmography, it is worth introducing some particular cosmographic parameters as follows:

$$j = \frac{a^{III}}{aH^3}, \quad s = \frac{a^{IV}}{aH^4} \text{ and } l = \frac{a^V}{aH^5},$$

whose values for our model are given by:

$$\text{jerk}(j) = 1 + 9e^{-2\gamma_1 t} \gamma_2^2; \tag{32}$$

$$\text{snap}(s) = 1 + 9e^{\gamma_1 t} \gamma_2 - 45e^{-2\gamma_1 t} \gamma_2^2 + 27e^{-3\gamma_1 t} \gamma_2^3; \tag{33}$$

$$\text{lerk}(l) = 1 - 6e^{-\gamma_1 t} \gamma_2 + 306e^{-2\gamma_1 t} \gamma_2^2 - 486e^{-3\gamma_1 t} \gamma_2^3 + 81e^{-4\gamma_1 t} \gamma_2^4 \tag{34}$$

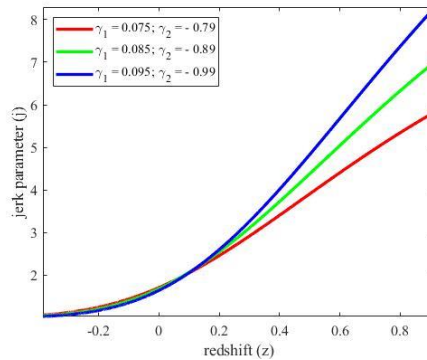


Figure 9: Illustration of jerk parameter(j) against redshift(z).

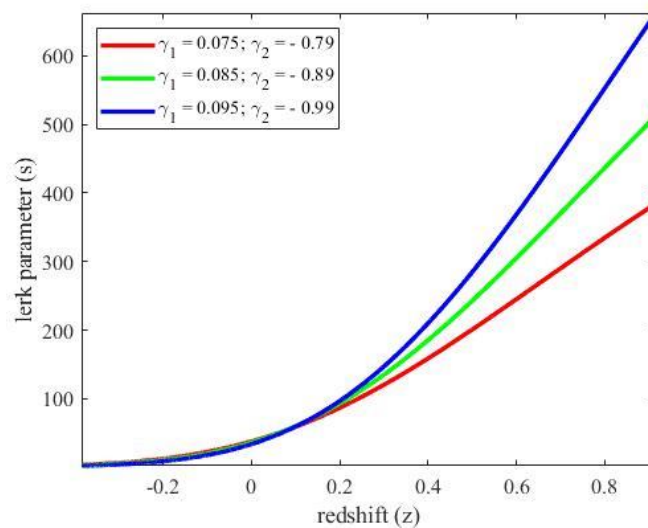


Figure 10: Illustration of lerk parameter(l) against redshift(z).

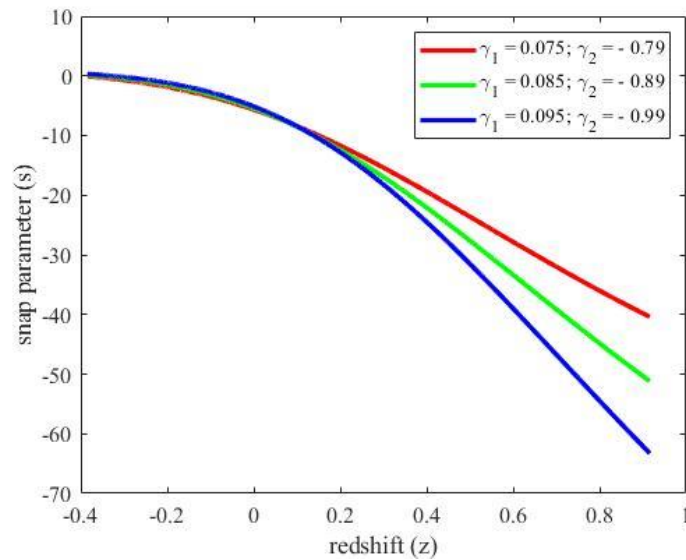


Figure 11: Illustration of snap parameter(s) against redshift(z).

The cosmographic parameters- jerk (j), lerk (l) and snap (s) for various values of γ_1 and γ_2 , plotted against redshift (z) are represented in figures (9), (10) and (11) respectively. For jerk and lerk parameters there is a variation in the positive region, whereas for the snap parameter, the sign changes from the erstwhile negative values to contemporary positive one, regardless of the values of γ_1 & γ_2 . These cosmographic parameters are in obedience to the present-time observations.

- **EoS Parameter (ω_{de}):** The behavior of DE phenomena is most commonly defined with the EoS parameter as, $\omega_{de} = \frac{p}{\rho_{de}}$, where p is pressure and ρ_{de} is energy density. The range of EoS parameter ω_{de} , when lies between $(-1, -\frac{1}{3})$ describes quintessence DE model. $\omega_{de} = -1$ gives the vacuum DE, usually called as cosmological constant or Λ CDM model and the DE model known as the phantom model is observed when $\omega_{de} < -1$. Inevitable singularity of space-time will result from this phantom DE model in the future. For our model the EoS parameter is given by:

$$\omega_{de} = \frac{\Psi_2}{2(2n+1)(e^{\gamma_1 t} + \gamma_2)^2}, \tag{35}$$

where,

$$\Psi_2 = \left. \begin{aligned} & -\gamma_2^3(n+3)(n+2)e^{-\gamma_1 t} + (-3n^2\gamma_2 - 7n\gamma_2 - 14\gamma_2)e^{\gamma_1 t} \\ & + (-3n^2 - 11n - 16)\gamma_2^2 - (n^2 + n + 4)e^{2\gamma_1 t}. \end{aligned} \right\}$$

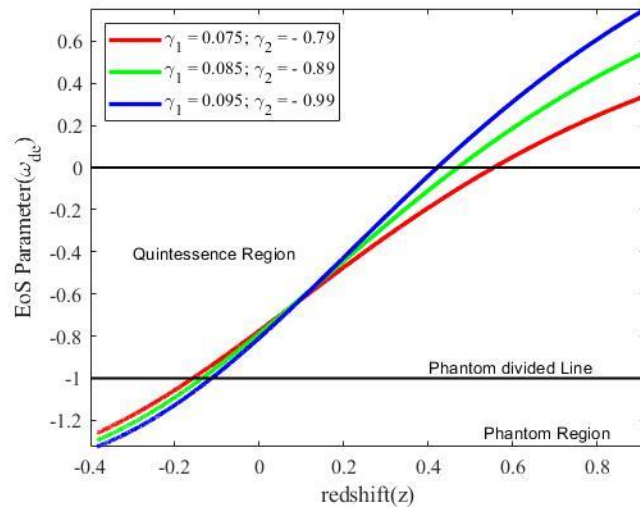


Figure 12: Illustration of EoS parameter(ω_{de}) against redshift(z).

For three values of γ_1 & γ_2 , the EoS parameter (ω_{de}) has been depicted against redshift (z) in the figure (12). The path of the EoS parameter has started from radiation dominated phase and moves towards quintessence region. After crossing the phantom divide line it reaches the phantom region. Such a behavior of the Universe is called as the quintessence nature. According to the obtained model, the observed EoS parameter matches the 2018 Planck data [4], where the EoS parameters limits are as follows:

$$\omega_{de} = \begin{cases} -1.56^{+0.60}_{-0.48} (\text{Planck} + \text{TT} + \text{loE}) \\ -1.58^{+0.52}_{-0.41} (\text{Planck} + \text{TT}, \text{EE} + \text{loE}) \\ -1.57^{+0.50}_{-0.40} (\text{Planck} + \text{TT}, \text{TE}, \text{EE} + \text{loE} + \text{lensing}) \\ -1.04^{+0.10}_{-0.10} (\text{Planck} + \text{TT}, \text{TE}, \text{EE} + \text{loE} + \text{lensing} + \text{BAO}) \end{cases}$$

• **$\omega_{de} - \omega_{de}'$ plane:** First and foremost, Cadwell and Linder [56] have proposed the EoS plane to explain the regions of the expanding Universe for evaluating the quintessence scalar field. The plane characterizes two distinct regions for different values of ω_{de} and ω_{de}' (where ' represents differentiation w.r.t $\ln a$). The plane is referred as thawing region, whenever $\omega_{de}' > 0$, $\omega_{de} < 0$ and freezing region for $\omega_{de}' < 0$, $\omega_{de} < 0$. The ω_{de}' is given by :

$$\omega_{de}' = \frac{3\gamma_2(e^{-2\gamma_1 t} \gamma_2^6 + 6e^{-\gamma_1 t} \gamma_2^5 + 15\gamma_2^4 + 20e^{\gamma_1 t} \gamma_2^3 + 15e^{2\gamma_1 t} \gamma_2^2 + 6e^{3\gamma_1 t} \gamma_2 + e^{4\gamma_1 t})(n+3)(n+2)}{2(2n+1)(e^{\gamma_1 t} + \gamma_2)^5} \tag{36}$$

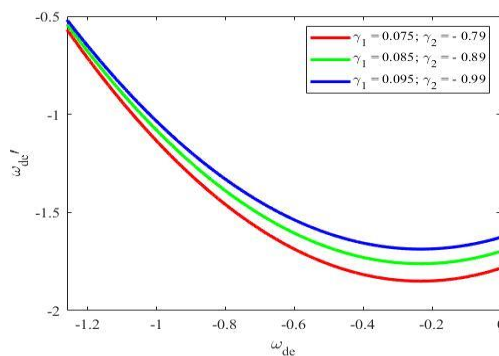


Figure 13: Illustration of EoS plane ($\omega_{de} - \omega_{de}'$)

Figure (13) represents the EoS plane ($\omega_{de} - \omega_{de}'$) for this cosmological model, for various values of γ_1 & γ_2 . It is observed that the model lies in freezing region as $\omega_{de}' < 0$ & $\omega_{de} < 0$ for our BHDE model. This represents an accelerating cosmic expansion. The trajectories of $\omega_{de} - \omega_{de}'$ plane, in the model converge with the experimental data [57,58],

$$\omega_{de} = -1.17^{+0.13}_{-0.12}, \omega_{de}' = 0.85^{+0.50}_{-0.49}(\text{WMAP} + \text{eCAMB} + \text{BAO} + H_0 + \text{SNe}).$$

$$\omega_{de} = -1.13^{+0.24}_{-0.25}, \omega_{de}' < 1.32(\text{Planck} + \text{WP} + \text{BAO}).$$

$$\omega_{de} = -1.34^{+0.18}_{-0.18}, \omega_{de}' = 0.85 \pm 0.7(\text{WMAP} + \text{eCAMB} + \text{BAO} + H_0).$$

• **Stability Analysis:** The squared speed of sound (v_s^2) examines the model's stability and is defined as the partial derivative of pressure w.r.t density as, $\frac{\dot{p}_{de}}{\dot{\rho}_{de}}$ [59,60]. For the developed model, the stability is defined from the following value of v_s^2 ,

$$v_s^2 = \frac{\Psi_3}{4(n+\frac{1}{2})(\Delta-2)(e^{\gamma_1 t + \gamma_2})^6}, \tag{37}$$

where,

$$\Psi_3 = \left. \begin{aligned} & -\gamma_2^7(n+3)(n+2)(\Delta-3)e^{-\gamma_1 t} - 35((\Delta-3)n^2 + (\frac{23\Delta}{7} - \frac{81}{7})n + \frac{36\Delta}{7} - \frac{114}{7})\gamma_2^4 e^{2\gamma_1 t} \\ & - 35((\Delta-3)n^2 + (\frac{19\Delta}{7} - \frac{73}{7})n + \frac{34\Delta}{7} - \frac{110}{7})\gamma_2^3 e^{3\gamma_1 t} - 21\gamma_2^2((\Delta-3)n^2 + (\frac{15\Delta}{7} \\ & - \frac{65}{7})n + \frac{32\Delta}{7} - \frac{106}{7})e^{4\gamma_1 t} - 7((\Delta-3)n^2 + (\frac{11\Delta}{7} - \frac{57}{7})n + \frac{30\Delta}{7} - \frac{102}{7})\gamma_2 e^{5\gamma_1 t} \\ & - 21((\Delta-3)n^2 + (\frac{27\Delta}{7} - \frac{89}{7})n + \frac{38\Delta}{7} - \frac{118}{7})\gamma_2^5 e^{\gamma_1 t} + ((-7\Delta + 21)n^2 \\ & + (-31\Delta + 97)n - 40\Delta + 122)\gamma_2^6 - ((\Delta-3)n^2 + (\Delta-7)n + 4\Delta - 14)e^{6\gamma_1 t}. \end{aligned} \right\}$$

In figure (14) the squared speed of sound (v_s^2) has been depicted against redshift (z) for various values of γ_1 & γ_2 . The outlined plot is identified in the positive region giving a stable behavior for the Universe.

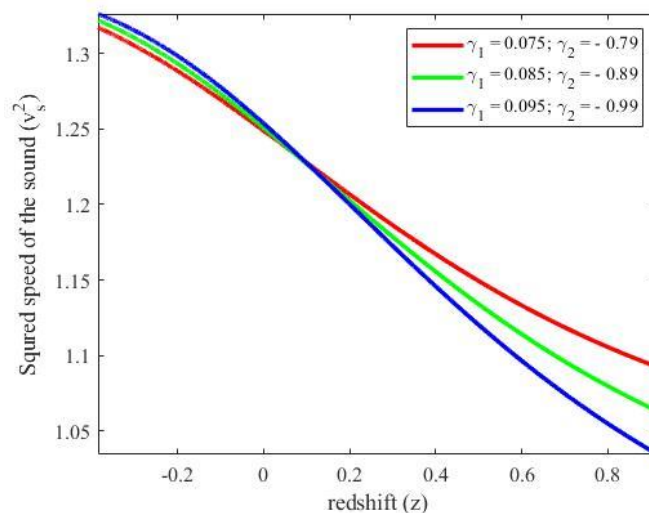


Figure 14: Illustrating of squared speed of sound(v_s^2) against redshift(z)

• **Density Parameter:** The dimensionless density parameter of DE (Ω_{de}) is formulated as

$$\Omega_{de} = \frac{\rho_{de}}{3H^2}. \tag{38}$$

We were able to obtain the density parameter of DE for our BHDE model by substituting the expressions for the Hubble parameter (H) and the energy density (ρ_{de}) in the above equation;

and we used graphical representation to analyze its behavior. A detailed study about the density parameter has been already mentioned in the Section (1), whose value is given by

$$\Omega_{de} = \frac{27C(e^{\gamma_1 t} + \gamma_2)^4 e^{-4\gamma_1 t} \left(\frac{e^{\gamma_1 t}}{e^{\gamma_1 t} + \gamma_2}\right)^{\Delta_3 - \Delta}}{\gamma_1^4} \tag{39}$$

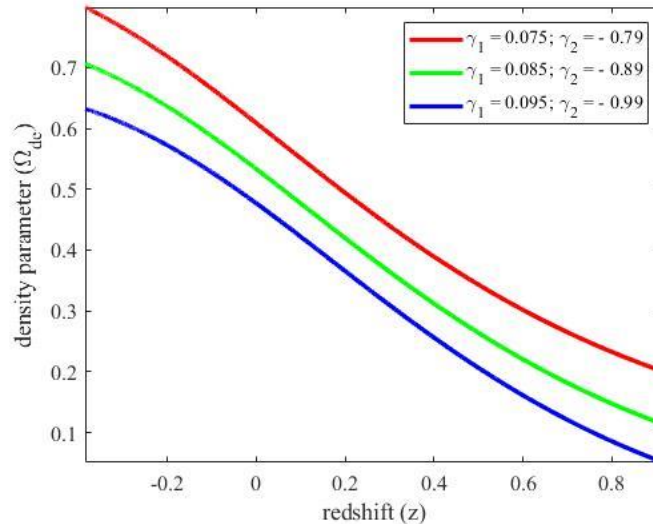


Figure 15: Illustration of density parameter (Ω_{de}) against redshift(z)

For distinct values of γ_1 & γ_2 , the plot for density parameter (Ω_{de}) has been constructed against redshift (z) in the figure (15). The trajectories of density parameter (Ω_{de}) vary in the positive region, increasing against redshift, satisfying the limits at the present epoch as mentioned below. Also, the BHDE density parameter satisfies the following limits at the present epoch. Observations from Planck’s data (2014)[57], the density parameter of DE, has taken the following limitations $\Omega_{de} = 0.717^{+0.028}_{-0.024}$ (WMAP-9) and $\Omega_{de} = 0.717^{+0.023}_{-0.020}$ (Planck+WP) and Planck’s data (2018) [4] have given the constraints on DE density parameter as $\Omega_{de} = 0.679 \pm 0.013$ (TT+loE), 0.6834 ± 0.0084 (TT,TE,EE+loE), 0.6847 ± 0.0073 (TT,TE,EE++loE+lensing), 0.6889 ± 0.0056 (TT,TE,EE++loE+lensing+BAO), 0.699 ± 0.012 (TT+loE), $0.711^{+0.033}_{-0.026}$ (EE+loE). Hinshaw et al. [58] have set forth limitation on density parameter Ω_{de} as $\Omega_{de} = 0.721 \pm 0.025$ (WMAP), $\Omega_{de} = 0.728 \pm 0.019$ (WMAP+eCMB), $\Omega_{de} = 0.707 \pm 0.010$ (WMAP+ eCMB+ BAO), $\Omega_{de} = 0.740 \pm 0.015$ (WMAP+eCMB+ H_0), $\Omega_{de} = 0.7135^{+0.0095}_{-0.0096}$ (WMAP+eCMB+BAO+ H_0).

4 Interpretations of the model:

We have constructed a BHDE model in the framework of SCT. It is observed from the construction of the plots, that the energy density BHDE (ρ_{de}), matter (ρ_m) and the pressure (p) projects the Universe’s expansion in an accelerated manner. Also the Hubble parameter shows that H is directly proportional to cosmic time (t) and the redshift (z) attaining its present value H_0 at $z = 0$. However, H is inversely proportional towards scale factor (a). The skewness parameter (δ) of the model differs in the positive region and does not vanish all over its evolution.

To understand the physical significance of the model, various cosmological parameter have been studied. The deceleration parameter (q) thus obtained, shows decelerated expansion during the erstwhile phases of the Universe, and later on, the accelerated expansion phase is observed, that is concurrent with the recent astrophysical observations. The r, s plane and q, r plane trajectories projects that the constructed model behaves like a Λ CDM model; and illustrates the phase shift of the Universe from matter dominated phase to de-Sitter phase respectively. The cosmographic parameters are in coincidence with the latest astronomical observations as the lerk (l) and jerk (j) parameters varies in positive region and the snap parameter (s) changes its sign from negative to positive ones. The EoS parameter of the model states that the Universe has a quintessence nature and the trajectories of the EoS plane ($\omega_{de} - \omega_{de}'$) lies in the freezing region, both representing accelerating cosmic expansion. The Universe shows a stable behavior as the parameter v_s^2 varies in the positive region. The density parameter (Ω_{de}) obtained is consistent with the recent observations, as its trajectories are varying in the positive region. Hence, the model built, behaves like a Λ CDM model, showing a stable behavior; having quintessence nature and further illustrates that, the Universe is expanding in an accelerated manner. These observations are in good agreement with the recent experimental data.

References

1. Robert R Caldwell and Michael Doran. Cosmic microwave background and supernova constraints on quintessence: concordance regions and target models. *Phys.Rev.D*, 69(10):103517, 2004.
2. Zhuo-Yi Huang, Bin Wang, Elcio Abdalla, and Ru-Keng Su. Holographic explanation of wide- angle power correlation suppression in the cosmic microwave background radiation. *J. Cosmol. Astropart. Phys.*, 2006(05):013, 2006.
3. Davide Castelvecchi et al. New type of dark energy could solve Universe expansion mystery.
4. *Nature*, 597(7877):460–461, 2021.
5. Nabila Aghanim, Yashar Akrami, Mark Ashdown, J Aumont, C Baccigalupi, M Ballardini, AJ Banday, RB Barreiro, N Bartolo, S Basak, et al. Planck 2018 results-VI. Cosmological parameters. *Astronomy & Astrophysics*, 641:A6, 2020.
6. Saul Perlmutter, Goldhaber Aldering, Gerson Goldhaber, RA Knop, Peter Nugent, Patricia G Castro, Susana Deustua, Sebastien Fabbro, Ariel Goobar, Donald E Groom, et al. Measurements of Ω and Λ from 42 high-redshift supernovae. *Astrophys.J.*, 517(2):565, 1999.
7. Adam G Riess, Alexei V Filippenko, Peter Challis, Alejandro Clocchiatti, Alan Diercks, Peter M Garnavich, Ron L Gilliland, Craig J Hogan, Saurabh Jha, Robert P Kirshner, et al. Observational evidence from supernovae for an accelerating universe and a cosmological constant. *Astron.J.*, 116(3):1009, 1998.
8. Davide Castelvecchi. Mystery over Universe's expansion deepens with fresh data. *Nature*, 583(7817):500–502, 2020.
9. Gerard't Hooft. Dimensional reduction in quantum gravity. arXiv preprint gr-qc/9310026, 1993.
10. Arellano-Zubiate, J. ., J. . Izquierdo-Calongos, A. . Delgado, and E. L. . Huamaní. "Vehicle Anti-Theft Back-Up System Using RFID Implant Technology". *International Journal on*

Recent and Innovation Trends in Computing and Communication, vol. 10, no. 5, May 2022, pp. 36-40, doi:10.17762/ijritcc.v10i5.5551.

11. Leonard Susskind. The world as a hologram. *J.Math.Phys.*, 36(11):6377–6396, 1995.
12. Willy Fischler and Leonard Susskind. Holography and cosmology. arXiv preprint hep-th/9806039, 1998.
13. Andrew G Cohen, David B Kaplan, and Ann E Nelson. Effective field theory, black holes, and the cosmological constant. *Phys. Rev. Lett.*, 82(25):4971, 1999.
14. Petr Horava and Djordje Minic. Probable values of the cosmological constant in a holographic theory. *Phys.Rev.Lett.*, 85(8):1610, 2000.
15. Raphael Bousso. The holographic principle. *Rev.Mod.Phys.*, 74(3):825, 2002.
16. Shuang Wang, Yi Wang, and Miao Li. Holographic dark energy. *Physics reports*, 696:1–57, 2017.
17. JD Bekenstein. Black holes and entropy. *Phys. Rev. D*, 737:2333, 1972.
18. JD Bekenstein. Black holes and entropy. *Phys. Rev. D*, 7:2333, 1973.
19. Stephen W Hawking. Gravitational radiation from colliding black holes. *Phys. Rev. Lett.*, 26(21):1344, 1971.
20. Stephen W Hawking. Black holes in general relativity. *Commun. Math. Phys.*, 25(2):152–166, 1972.
21. Bikash Chandra Paul, Bikash Chandra Roy, and Arindam Saha. Bianchi-I anisotropic universe with Barrow holographic dark energy. *Eur. Phys. J. C*, 82(1):1–7, 2022.
22. Abdulla Al Mamon, Andronikos Paliathanasis, and Subhajit Saha. Dynamics of an interacting Barrow holographic dark energy model and its thermodynamic implications. *Eur. Phys. J. P.*, 136(1):1–14, 2021.
23. Philip, A. M., and D. S. Hemalatha. “Identifying Arrhythmias Based on ECG Classification Using Enhanced-PCA and Enhanced-SVM Methods”. *International Journal on Recent and Innovation Trends in Computing and Communication*, vol. 10, no. 5, May 2022, pp. 01-12, doi:10.17762/ijritcc.v10i5.5542.
24. A Remya, Pankaj, and Umesh Kumar Sharma. Cosmological parameters in Barrow holographic dark energy. *Int. J.Geom. Met. Mod. Phys.*, 19(06):2250082, 2022.
25. Priyanka Adhikary, Sudipta Das, Spyros Basilakos, and Emmanuel N Saridakis. Barrow holographic dark energy in a nonflat universe. *Phys. Rev. D*, 104(12):123519, 2021.
26. Shamaila Rani and Nadeem Azhar. Braneworld inspires cosmological implications of barrow holographic dark energy. *Universe*, 7(8):268, 2021.
27. Vinod Kumar Bhardwaj, Archana Dixit, and Anirudh Pradhan. Statefinder hierarchy model for the Barrow holographic dark energy. *New Astronomy*, 88:101623, 2021.
28. George Lemaître. A homogeneous Universe of constant mass and increasing radius accounting for the radial velocity of extra-galactic nebulae. In *Ann. Sci. Soc.Bru.*, volume 47, pages 49–59, 1927.
29. Knut Lundmark. The motions and the distances of spiral nebulae. *Mon. Not. R. Astron. Soc*, 85:865, 1925.
30. Edwin Hubble. A relation between distance and radial velocity among extra-galactic nebulae. *Proc. Nat. Acad. Sci.*, 15(3):168–173, 1929.
32. Wei-Tou Ni. Empirical foundations of the relativistic gravity. *Int. J. Mod. Phys. D*, 14(06):901–

921, 2005.

33. Clifford M Will. The confrontation between general relativity and experiment. *Living Rev. Relativ.*, 17(1):1–117, 2014.
34. Nouby M. Ghazaly, A. H. H. . (2022). A Review of Using Natural Gas in Internal Combustion Engines. *International Journal on Recent Technologies in Mechanical and Electrical Engineering*, 9(2), 07–12. <https://doi.org/10.17762/ijrmee.v9i2.365>
35. Slava G Turyshev. Experimental tests of general relativity: recent progress and future directions.
36. *Physics-Uspekhi*, 52(1):1, 2009.
37. Abhay Ashtekar. 100 Years of Relativity: Space-Time Structure-Einstein and Beyond. World Scientific, 2005.
38. T Padmanabhan. One hundred years of General Relativity: Summary, status and prospects.
39. *Curr. Sci.*, 109(7):1215–1219, 2015.
40. Garth A Barber. On two “self-creation” cosmologies. *Gen. Rel. Grav.*, 14(2):117–136, 1982.
41. Carl Brans and Robert H Dicke. Mach’s principle and a relativistic theory of gravitation. *Phys. Rev.*, 124(3):925, 1961.
42. Shri Ram, S Chandel, and MK Verma. Kantowski-Sachs Model with Modified Holographic Ricci Dark Energy in Self-Creation Theory of Gravitation. *Prespacetime Journal*, 11(6), 2020.
43. NK Ashtankar, MS Borkar, VM Raut, and NP Gaikwad. LRS Bianchi type-II bulk viscous string cosmological model in Barber’s second self-creation theory. *Vidya.Int.Interdis. Res. J.*, 10:110, 2020.
44. Pawan Kumar Tiwari, Mukesh Kumar Yadav, R. K. G. A. . (2022). Design Simulation and Review of Solar PV Power Forecasting Using Computing Techniques. *International Journal on Recent Technologies in Mechanical and Electrical Engineering*, 9(5), 18–27. <https://doi.org/10.17762/ijrmee.v9i5.370>
45. Vimal C Jain and Nikhil Jain. Bianchi type VI₀ Dark Energy Models with Constant Deceleration Parameter in Self-Creation Cosmology. *Prespacetime Journal*, 12(1):42, 2021.
46. Dinkar Singh Chauhan. LRS Bianchi Type-I Models in Self-Creation Cosmology. *Research Guru*, 15, 2021.
47. SC Wankhade, AS Nimkar, and AM Pund. Wet Dark Fluid Cosmological Model in Barber Self-Creation Theory of Gravitation. *J.Sci.Res.*, 13(3):869–878, 2021.
48. Priya Advani. Cosmological Model of Bianchi Type-V in Perfect Fluid and Lyra Geometry with Self-Creation Theory of Gravitation. *Prespacetime Journal*, 12(3), 2021.
49. Priya Advani and Nikhil Jain. Cosmological Model of Bianchi Type-I Involving Magnetic Radiation in Self-Creation Theory of Gravitation with Constant Deceleration Parameter. *Prespacetime Journal*, 12(5), 2021.
50. Garg, D. K. . (2022). Understanding the Purpose of Object Detection, Models to Detect Objects, Application Use and Benefits. *International Journal on Future Revolution in Computer Science & Communication Engineering*, 8(2), 01–04. <https://doi.org/10.17762/ijfrcsce.v8i2.2066>
51. R Kumar and S Arora. Bi-Quadratic Varying Deceleration Parameter to Study the Cosmological Model. In *J. Phys.: Conf. Series*, volume 2267, page 012138. IOP Publishing, 2022.
52. Archana Dixit, Shilpi Singhal, and Mohd Zeyauddin. Model for Modified Holographic Ricci Dark Energy in Gravitation Theory of Branc Dicke. *Walailak J. Sci. & Tech.*, 18(3):6986–15,

2021.

53. GK Goswami, Meena Mishra, Anil Kumar Yadav, and Anirudh Pradhan. Two-fluid scenario in Bianchi type-I universe. *Mod. Phys. Lett. A*, 35(12):2050086, 2020.
54. Hassan Amirhashchi and Soroush Amirhashchi. Constraining Bianchi type I universe with type Ia supernova and $H(z)$ data. *Phys. Dark Uni.*, 29:100557, 2020.
55. Nishant Singla, Anil Kumar Yadav, MK Gupta, GK Goswami, and Rajendra Prasad. Probing kinematics and fate of Bianchi type I universe in Brans–Dicke theory. *Mod. Phys. Lett. A*, 35(21):2050174, 2020.
56. RV Maluf and Juliano Neves. Bianchi type I cosmology with a Kalb–Ramond background field. *Eu. Phys. J. C*, 82(2):1–9, 2022.
57. CB Collins, EN Glass, and DA Wilkinson. Exact spatially homogeneous cosmologies. *Gen. Relativ. Gravit.*, 12(10):805–823, 1980.
58. Rishi Kumar Tiwari and Değer Sofuoğlu. Quadratically varying deceleration parameter in $f(R, T)$ gravity. *Int. J. Geom. Methods Mod. Phys.*, 17(10):2030003, 2020.
59. RK Tiwari, Değer Sofuoğlu, and VK Dubey. Phase transition of LRS Bianchi type-I cosmological model in $f(R, T)$ gravity. *Int. J. Geom. Methods Mod. Phys.*, 17(12):2050187, 2020.
60. N Hulke, GP Singh, Binaya K Bishi, and Ashutosh Singh. Variable Chaplygin gas cosmologies in $f(R, T)$ gravity with particle creation. *New Astronomy*, 77:101357, 2020.
61. GP Singh, N Hulke, and Ashutosh Singh. Cosmological study of particle creation in higher derivative theory. *Indian J. Phys.*, 94(1):127–141, 2020.
62. Varun Sahni, Tarun Deep Saini, Alexei A Starobinsky, and Ujjaini Alam. Statefinder—a new geometrical diagnostic of dark energy. *J. Exp. Theor. Phys. Lett.*, 77(5):201–206, 2003.
63. Ujjaini Alam, Varun Sahni, Tarun Deep Saini, and AA Starobinsky. Exploring the expanding universe and dark energy using the Statefinder diagnostic. *Mon. Not. R. Astron. Soc.*, 344(4):1057–1074, 2003.
64. Varun Sahni, Arman Shafieloo, and Alexei A Starobinsky. Two new diagnostics of dark energy. *Phys. Rev. D*, 78(10):103502, 2008.
65. RR Caldwell and Eric V Linder. Limits of quintessence. *Phys. R. Lett.*, 95(14):141301, 2005.
66. Peter AR Ade, Nabila Aghanim, Charmaine Armitage-Caplan, Mark Arnaud, M Ashdown, F Atrio-Barandela, J Aumont, C Baccigalupi, Anthony J Banday, RB Barreiro, et al. Planck 2013 results. XVI. Cosmological parameters. *Astro. & Astrophys.*, 571:A16, 2014.
67. Gary Hinshaw, D Larson, Eiichiro Komatsu, David N Spergel, CLaa Bennett, Joanna Dunkley, MR Nolta, M Halpern, RS Hill, N Odegard, et al. Nine-year Wilkinson Microwave Anisotropy
68. Probe (WMAP) observations: cosmological parameter results. *Astrophys J. Suppl.*, 208(2):19, 2013.
69. Kyoung Yee Kim, Hyung Won Lee, and Yun Soo Myung. Instability of agegraphic dark energy models. *Phys. Lett. B*, 660(3):118–124, 2008.
70. M Sharif and Abdul Jawad. Cosmological evolution of interacting new holographic dark energy in non-flat universe. *Eur. Phys. C*, 72(8):1–9, 2012.